Prewetting transitions of one site associating fluids

Sandip Khan and Jayant K. Singh

Citation: J. Chem. Phys. **132**, 144501 (2010); doi: 10.1063/1.3382345
View online: http://dx.doi.org/10.1063/1.3382345
View Table of Contents: http://jcp.aip.org/resource/1/JCPSA6/v132/i14
Published by the AIP Publishing LLC.

Prewetting transitions of one site associating fluids

Sandip Khan and Jayant K. Singh[a)]
Department of Chemical Engineering, Indian Institute of Technology Kanpur, Kanpur 208016, India

(Received 26 November 2009; accepted 16 March 2010; published online 8 April 2010)

Prewetting transitions are studied for Lennard-Jones (LJ) based dimer forming associating fluids, on a structureless surface represented by LJ 9–3 type potential, for various association strengths using grand-canonical transition matrix Monte Carlo (GC-TMMC) and histogram reweighting techniques. Occurrences of prewetting transition are observed for association strengths: ε_{af}=2.0, 4.0, 6.0, 8.0, and 10.0. Structural properties, monomer fraction, and orientation order profile of thin-thick film of one-site associating fluids are presented. Wetting temperature, T_w, and prewetting critical temperature, T_{pwc}, increases with increasing association strength, which is in agreement with the results of the density functional theory (DFT). Length of prewetting line, on the other hand, is found to decrease first with increasing association energy until ε_{af}=8.0 and subsequently found to increase substantially for ε_{af}=10. This behavior is contrary to the prediction from the DFT. We observe that the boundary tension of thin-thick film via GC-TMMC and finite size scaling exhibits a maximum with respect to association strength. © *2010 American Institute of Physics*. [doi:10.1063/1.3382345]

I. INTRODUCTION

Understanding the structural and dynamical properties of associating fluids is important not only to biological processes but also for various industrial processes. It was seminal papers of Wertheim,[1,2] which put the first sound model of association based on statistical mechanics. Subsequent to that, Chapman,[3] Gubbins and co-workers,[4–6] and Huang and Radosz[7,8] have reformulated the work and presented in the form of statistical associating fluid theory (SAFT). Since, then variants such as SAFT,[5,9] SAFT-LJ,[10–12] copolymer SAFT,[13] soft SAFT,[14,15] SAFT-VR,[16,17] SAFT1,[18] and PC-SAFT[19] are in existence and have been very successful in the prediction of the bulk properties of associating fluids. In addition to the bulk properties, SAFT[20,21] has been modified to predict interfacial properties. Molecular simulation, on the other hand, is more successful in accurate prediction of phase equilibria of model associating fluids; however, at higher association strengths, biasing techniques are essential for proper sampling of the phase space.[22–24] Due to inherent problems associated with sampling of associating fluids, molecular simulation of highly associating fluids is still difficult, which is evident from relatively very less number of articles published in this area.[25–27]

Associating fluids are usually modeled as a system of spherical particles with short range directional interaction. Such patchy interaction recently has been used also in the context of self assembly process of colloidal and biological fluids.[28–30] These fluids near surfaces are increasingly being studied due to the urgent need for molecular insight of the behavior of these fluids for the development of microfluidic devices.[31] Phase behavior near surfaces have been studied for simple fluids using various techniques and found to be extremely rich.[32] Relative strengths of surface-fluid and fluid-fluid interactions can lead to various phase transitions such as prewetting, wetting, layering, and capillary condensation.[32,33] Wetting transition is closely associated with a temperature called wetting temperature, T_w, at which adsorption state transforms from *partial wetting* to *complete wetting*. Below the wetting temperature, the thickness of the film adsorbed on a surface remains finite at all sub saturation pressures. Above wetting temperature prewetting transition, a first order transition, might be observed between two surface phase states differed by thickness of the adsorbed film. This prewetting transition stems from the saturation curve at the wetting temperature and terminates at prewetting critical point, T_{pwc}, where thin and thick films (surface phase states) become indistinguishable. In 1977, Cahn[34] predicted the existence of wetting transition for a two-phase mixture of fluids near a third phase, surface. Independently, Ebner and Saam[35] also predicted wetting and prewetting transition of a argon film adsorbed onto a weakly attractive solid carbon-dioxide surface using density functional theory (DFT). Experimental evidences, which came much later, support the prediction of prewetting transitions. Examples can be found for helium adsorption on Cs,[36,37] Rb,[38] liquid hydrogen on various substrates,[39] and acetone on graphite.[40]

In addition to theoretical and experimental findings, molecular simulation is increasingly employed among these studies due to its capability of detailed molecular description on the behavior. First order wetting transition such as prewetting transition is usually very close to the bulk gas-liquid coexistence line. Hence, simulations are difficult to conduct especially near T_w. Finn and Monson[41] were first to study the prewetting transition of argon molecules on solid carbon-dioxide system using isobaric Monte Carlo (MC) method. Subsequently, few more groups have utilized different molecular simulation methodologies[42–44] to understand the prewetting transition. Prediction on the coexistence of the thin-thick film has become efficient with the advent of ad-

[a)]Author to whom correspondence should be addressed. Electronic mail: jayantks@iitk.ac.in.

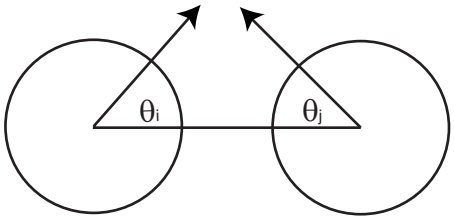

FIG. 1. Schematic diagram of single site associating model.

vanced simulation techniques such as grand-canonical transition matrix MC (GC-TMMC),[45,46] multicanonical sampling,[47] and histogram reweighting.[48] Errington[49] recently revisited the prewetting transitions of model argon on solid carbon dioxide, and further successfully demonstrated the use of GC-TMMC to predict the wetting temperature[49] and boundary tension.[50] On the other hand, prewetting behavior of associating fluids near surfaces though a common class of fluids in nature is not well studied. To our best knowledge, very limited molecular simulations are conducted to estimate wetting temperature and boundary tension of associating fluids.[51,52] This work primarily is motivated by the experimental evidence of prewetting behavior of acetone on graphite[40] and simulation observation of prewetting transition of water under confinement[53,54] and near the graphite surface.[55] This work presents a systematic investigation of prewetting transitions of one site model of associating fluids using GC-TMMC approach. The rest of the paper is organized as follows. Section II describes the models and methodologies used in this study. Simulation details are in Sec. III. Section IV presents the results and discussion followed by the conclusion in Sec. V.

II. MODEL AND METHODOLOGY

A. Model

In this work, we have used a model due to Chapman,[3] where Lennard-Jones (LJ) potential is used for isotropic van der Waals interactions. The model is depicted in Fig. 1. Off-center sites represent the association and are modeled using an orientationally dependent square-well attraction. These sites mimic the strong and short range directional attraction of real associating fluids. The complete potential used in this work is

$$u_{ff}(r_{ij},\theta_i,\theta_j) = u_{LJ-tr}(r_{ij}) + u_{\mathrm{af}}(r_{ij},\theta_i,\theta_j),$$

$$u_{\mathrm{af}}(r_{ij},\theta_i,\theta_j) = \begin{cases} -\varepsilon_{\mathrm{af}} & \text{if } r_{ij} < r_c, \\ & \theta_i < \theta_c \text{ and } \theta_j < \theta_c \\ 0 & \text{otherwise,} \end{cases}$$

$$u_{LJ-tr}(r_{ij}) = \begin{cases} 4\varepsilon\left[\left(\frac{r_{ij}}{\sigma}\right)^{12} - \left(\frac{r_{ij}}{\sigma}\right)^{6}\right] & \text{if } r_{ij} \le r_{\mathrm{cut}}, \\ 0 \text{ otherwise,} \end{cases} \tag{1}$$

where θ_i and θ_j (see Fig. 1) are angles between the center to center vector and the center to site vector of molecules i and j, respectively. $\varepsilon_{\mathrm{af}}$ is the association well depth and r_c is the range of associating potential. σ and ε are the molecular size and energy parameter of LJ potential. r_{cut} is the cutoff diameter for the LJ potential. All variables reported in this study are made dimensionless using σ and ε. For example, temperature, density, pressure and surface tension are reduced by ε/k, σ^{-3}, ε/σ^3 and ε/σ^2, respectively. In this study, θ_c, r_c and r_{cut} are fixed at 27°, 1.00, and 2.5, respectively.

In this work, a structureless and smooth substrate is used. Substrate-fluid molecular interaction at a distance z is specified by a LJ 9–3 potential:

$$u_{wf}(z) = \frac{2\pi}{3}\rho_{\mathrm{w}}\sigma_{\mathrm{w}}^3\varepsilon_{\mathrm{w}}\left[\frac{2}{15}\left(\frac{\sigma_{\mathrm{w}}}{z}\right)^9 - \left(\frac{\sigma_{\mathrm{w}}}{z}\right)^3\right], \tag{2}$$

where $\rho_{\mathrm{w}}\sigma_{\mathrm{w}}^3$, $\varepsilon_{\mathrm{w}}/\varepsilon$, and $\sigma_{\mathrm{w}}/\sigma$ are set to 0.988, 1.2771, and 1.0962, respectively, which corresponds to the argon-solid CO_2 system introduced by Ebner and Saam.[12]

B. Methodology

Prewetting transition can be investigated via molecular dynamics or MC slab based techniques as shown in our earlier work.[56,57] Such investigation is not most suited for phase transition near surface since appropriate gas density should be known beforehand to obtain surface phase transitions using slab based technique. Without proper density information, it is usually a time consuming investigation. In addition, it is rather tricky to distinguish between quasi-two-dimensional vapor-liquid transition and prewetting transition without any knowledge of chemical potential. GC-TMMC along with histogram reweighting,[48] on the other hand, is more suitable selection for such investigation. Details of GC-TMMC simulation techniques are given elsewhere.[49,50] However, for the sake of completeness, we provide a brief description of the methodology. GC-TMMC simulations are conducted in a grand-canonical ensemble at a constant chemical potential μ, volume V, and temperature T. Microstate probability in this ensemble is represented as

$$\pi_s = \frac{1}{\Xi}\frac{V^{N_s}}{\Lambda^{3N_s}N_s!}\exp[-\beta(U_s - \mu N_s)], \tag{3}$$

where $\beta = 1/k_{\mathrm{B}}T$ is the inverse temperature and k_{B} is the Boltzmann's constant, Ξ is the grand canonical partition function, U_s is the interaction energies of particles of microstate s, and Λ is the de Broglie wavelength.

In GC-TMMC simulations, three basic MC moves are used namely displacement, insertion and deletion moves. However, for associating fluids, we include bias MC and rotation moves also.[24,58] During moves, attempted transitions between microstates of different densities are monitored. At regular intervals during a simulation, this information is used to obtain an estimate of the density probability distribution, which is subsequently used to bias the sampling toward low probability densities using multicanonical sampling method.[47] Over time all densities of interest are sampled adequately. The final result is an efficient self-adaptive method for determining the density probability distribution over a specified range of densities. Once a probability distribution has been collected at a given value of chemical potential, histogram reweighting[48] is used to shift the probability distribution to other values of the chemical potential. Coexist-

ence chemical potential is calculated by recursively applying histogram reweighting[48] technique until we obtain a probability distribution, Π_N^{coex}, such that area under the thin and thick film regions in the probability distribution plot are equal. Densities of phases are calculated from the first moment of Π_N^{coex} distribution.

Thin and thick films associated with prewetting transition are known to be quasi-two-dimensional in nature.[35,59] The inhomogeneity in the boundary line between surface and coexisting phases gives rise to excess free energy. This excess free energy per unit length of boundary line is termed as boundary tension. Boundary tension, in this work, is calculated using GC-TMMC along with the finite-size scaling approach, as described by previous workers.[50] The interfacial energy for a finite-size system with a substrate length, L, is determined from the maximum likelihood in the thick film Π_{max}^{thick} and thin film regions Π_{max}^{thin} and minimum likelihood in the interface region Π_{min},

$$\beta F_L = \tfrac{1}{2}(\ln \Pi_{max}^{thin} + \ln \Pi_{max}^{thin}) - \ln \Pi_{min} \tag{4}$$

The interfacial free-energy of thin-thick film on a two dimensional surface varies with the system size according to the Binder's formalism[60] and is given by

$$\beta\tau_L = \frac{\beta F_L}{2L} = C_1\frac{1}{L} + C_2\frac{\ln(L)}{L} + \beta\tau, \tag{5}$$

where τ_L is the interfacial tension for a system of box length L, τ is the boundary tension for infinite system, C_1 and C_2 are constants, and F_L represents the free energy of the thin-thick interface for a finite system size L.

III. SIMULATION DETAILS

Bulk simulations are carried out in a cubic cell with cell length 6 and 8 to obtain the bulk saturation chemical potential. Cell length 6 is used only for lower temperature systems. Simulation box for prewetting transition simulations is periodic in two dimensions. The confined dimension is composed of an attractive surface, substrate, and the other end is the hard wall. Space between walls, height of the simulation box, is much larger than the substrate edge length. Different heights 20, 40, 80, and 120 are used for lower temperatures to ensure that hard wall has no affect on the properties. Phase diagram is calculated using substrate area, 9×9. Substantial larger substrate area, 12×12, is used at higher temperature closer to prewetting critical temperature to avoid system size effect on the phase transition.

In this work, trials were performed with probability 0.1, 0.35, 0.35, 0.1, and 0.1 for displacement, addition, deletion, rotation, and bias moves, respectively. Unbonding-bonding technique[24] is used to enhance the sampling. Further, multicanonical sampling technique is employed to force the system to sample the low probability states. Multiple cores (8–32) are used following the procedure employed by earlier workers.[49,58] Such possibility in splitting the transition matrix among different cores is particularly an attractive part of the GC-TMMC methodology, which allows sampling all the important phase states leading to efficient calculation of phase equilibria. However, more intelligent algorithms are required to overcome sampling issues at low temperatures closer to T_w for higher associating strengths. Boundary tension calculation is performed using finite size scaling with substrate areas 81, 144, 256, and 400. Corresponding maximum number of particles in the simulations ranges from 500 to 3000. In this work, we have performed around 1×10^9 to 8×10^{10} MC steps on 16 cores of Intel Xeon 2.66 GHz processor, depending on the associating strength, temperature, and substrate area. Four independent simulations are conducted to calculate the statistical error.

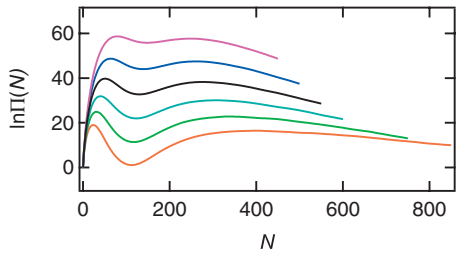

FIG. 2. The particle number probability distributions at coexistence for a series of temperatures for an associating fluid with $\varepsilon_{af}=6$. Curves from bottom to top are for $T=0.775$ through $T=0.90$ in increments of 0.025.

IV. RESULTS AND DISCUSSIONS

A. Phase diagram

We start our discussion with Fig. 2, which presents a set of typical coexistence particle number probability distributions for association fluid with $\varepsilon_{af}=6.0$. The phase coexistence behavior is akin to that seen for Ar–CO_2 system.[49] Binodal peaks are observed corresponding to the coexistence thin and thick films. The interfacial free energy, which is represented by the barrier between the peak and the trough, decreases with increasing temperature; and consequently, distinction between the two phases decreases and disappears at a temperature termed as critical prewetting temperature. Similar coexistence probability distributions are seen for other association strengths considered in this work.

As the prewetting transition is of first order transition, it can be characterized by separate phase diagram. The thick and thin films on the surface coexist with the bulk gas phase away from the surface. To evaluate the excess densities of the film, the bulk gas phase density needs to be calculated. However, it is an extensive exercise to obtain the bulk density away from the surface for the range of temperature of interest. Hence, we define the excess adsorption using the ideal gas approximation as also used earlier by few workers,[49]

$$N^{excess}(\mu) = \langle N(\mu)\rangle - \rho_b V \exp[\beta(\mu-\mu_b)], \tag{6}$$

where $\langle N(\mu)\rangle$ is the average number of particles and ρ_b and μ_b are the density and chemical potential of the bulk phase, respectively. The above expression can be compared with that from a more rigorous calculation. To this end, we have performed NVT simulations and obtained the bulk gas density away from the surface for subprewetting critical temperatures. It is found that error in using Eq. (6) varies with temperature. At extremely low temperature, the error is less than 1%. On the other hand, closer to prewetting critical

TABLE I. Wetting temperature, T_w, and critical prewetting temperature, T_{pwc}, for various association strength, ε_{af}. Errors associated with these temperatures are less than 1%.

ε_{af}	T_w	T_{pwc}	T_{bc}	T_w/T_{bc}	T_{pwc}/T_{bc}	$(T_{pwc}-T_w)/T_{bc}$
2	0.598	0.865	1.183	0.505	0.731	0.226
4	0.623	0.868	1.193	0.522	0.727	0.205
6	0.709	0.92	1.215	0.583	0.757	0.174
8	0.781	0.993	1.254	0.622	0.791	0.169
10	0.803	1.081	1.328	0.604	0.814	0.210

temperature the error is as high as 8%–14%. Nonetheless, increase in system size at higher temperature reduces the error to 1%–7%. Given this observation, we have used Eq. (6) to obtain the phase diagram and other properties with appropriate system size considerations. Since bulk chemical potential, μ_b, for the associating model of the current study has not been reported earlier, hence a series of GC-TMMC simulations are performed at temperatures of interest for the bulk associating fluid. Critical temperatures of the bulk associating fluids, calculated in this work, are reported in Table I.

Figure 3 presents the excess surface density of associating fluids with various association strengths. The effect of association is noticeable even at small association strengths as seen for $\varepsilon_{af}=4.0$. The general effect of association is to increase the density of the thick film and decrease the density of the thin film akin to that seen for bulk vapor-liquid associating fluids.[61] Increase in the thick film density with increase in association is attributed to the more compact arrangement of molecules; on the other hand, decrease in the thin film density is due to the lowering of coexistence pressure (pressure component parallel to the substrate and perpendicular to the thin-thick interface) with increasing association. The general effect of association is to raise the prewetting critical temperature. Though the thin-thick probability density distribution and phase diagram is quantitatively different from the bulk in shape, yet overall behavior is akin to that seen for bulk vapor-liquid phase coexistence of associating fluids.[58]

Figure 4(a) shows the density profile of thick and thin films at $T=0.85$ with different associating strengths. This temperature is close to the prewetting critical temperature ($T/T_{pwc}=0.98$) for $\varepsilon_{af}=4$; however, it is substantially subcritical ($T/T_{pwc}=0.86$) for $\varepsilon_{af}=8$. The number of molecular layers near the surface is sensitive to the association strength. In the case of thick film, we observed three to five layers with increasing ε_{af} at a given temperature. On the other hand, number of layers in the thin film decreases with increasing association strength and is limited to one to two for the range of association strength considered in the work. Furthermore, the density of each peak in the thick film also increases with increase in the ε_{af}. On the contrary, the density of each layer in thin film decreases with increasing association strength. Away from the surface, fluid behavior approaches to that of the bulk. However, the crossover from prewetting films to the bulk gas is dependent on the associating strength. For example, at $T=0.85$, thick film density, for $\varepsilon_{af}=4$, approaches the bulk value at $z\sim 7$. Conversely, for $\varepsilon_{af}=8$ the crossover occurs around $z\sim 12$. Figure 4(b) compares the local density for different temperature for $\varepsilon_{af}=6$. Similar to the behavior seen in Fig. 4(a), number of layers for thick film increases with decreasing temperature; on the other hand, layering is seen to reduce in the thin film with decreasing temperature mainly due to the decreased density at lower temperature.

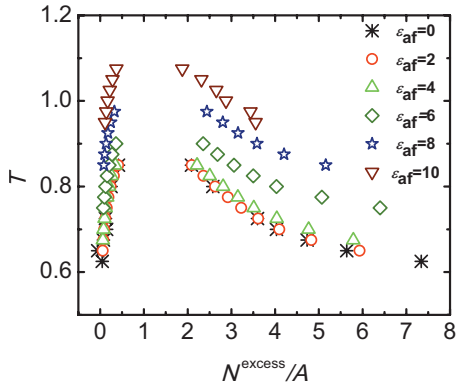

FIG. 3. Prewetting coexistence curves for different associating strengths. Statistical error is smaller than the symbol size.

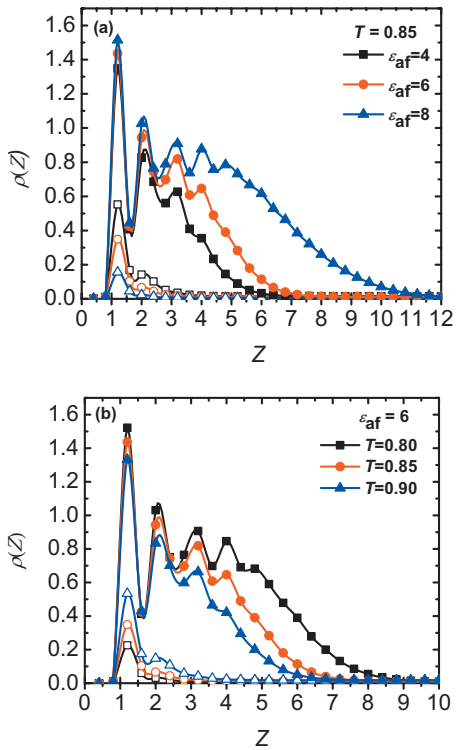

FIG. 4. Local density profile for coexistence thick and thin films: (a) at $T=0.85$, (b) for $\varepsilon_{af}=6$. Thick films are represented by the filled symbols whereas open symbols are for thin films.

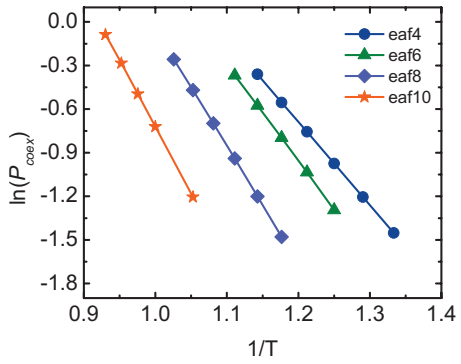

FIG. 5. Coexistence pressure of thin-thick film of associating fluids with different associating strengths as a function of the inverse of temperature.

Prewetting coexistence pressure (pressure component parallel to the surface and perpendicular to the thin-thick interface) between the two phases are also calculated in this work and plotted in Fig. 5 in a Clausius–Clapeyron form. Interestingly, the behavior is similar to seen for bulk saturation pressure.[58] The coexistence pressure of thin-thick film decreases with increasing association at a given temperature. Slope of the curve is connected primarily to the change in the enthalpy between thick and thin films, ΔH. Association in the thin film tends to diminish the ΔH, while that in the liquid increases it. That it increases with increasing association reflects a greater response of the thick film monomer fraction to increasing association strength, in comparison to the thin film. We specifically calculated the monomer fraction to verify this observation. Monomer fraction is determined by the fraction of total molecules which are in the nonbonded state. Figure 6 presents the monomer fraction of thin and thick films for various associating fluids. It is evident from Fig. 6 that monomer fraction in the thin film is not being affected significantly by the change in temperature particularly at lower association contrary to that seen for the thick film. Association strength, on the other hand, substantially influences the monomer fraction of thin and thick films. Monomer fraction, in general, is found to decrease with increasing association. Thin film is seen to be affected relatively more by increasing association strength beyond $\varepsilon_{af}=8$. A change in behavior is seen at higher association, $\varepsilon_{af}=10$, where difference in the monomer fraction in the two

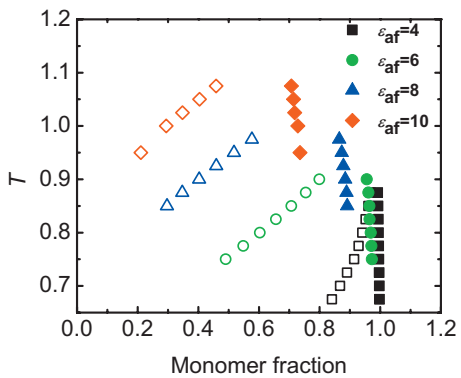

FIG. 6. Monomer fraction for coexistence thin and thick films for different association strengths. Filled symbols represent the thin film and open symbols represent the thick film. Error bars are smaller than the symbol size.

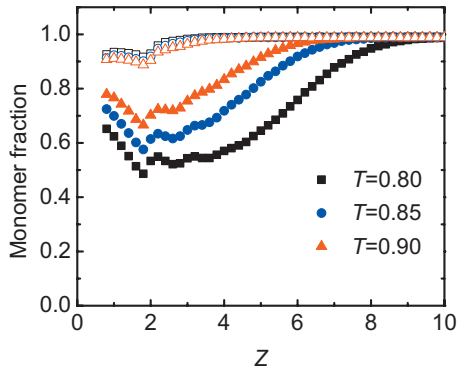

FIG. 7. Coexistence monomer fraction profile for thick and thin films of associating fluid with $\varepsilon_{af}=6$ at different temperatures. Filled symbols represent the thick film and open symbols represent the thin film.

phases seemingly saturates relative to that at $\varepsilon_{af}=8$ (not shown). This indicates a crossover behavior at higher association strength which would affect the interfacial properties as described later in this article. Figure 7 presents the monomer fraction profile for a typical association, $\varepsilon_{af}=6.0$. Monomer fraction profile as a function of distance from the substrate is oscillatory in nature. This behavior is not surprising as monomer fraction is dependent on the density, which possesses oscillatory behavior, as seen in Fig. 4. Hence, peaks and troughs in the monomer fraction profile correspond to the troughs and peaks of the density profile, respectively (see Fig. 4). It is noted that monomer fraction is not defined for $z<0.8$ as particles are not seen in that region which is also evident from Fig. 4.

Since associating molecules are anisotropic in nature, hence, it is expected that the orientation of the particles would be dependent on the density, temperature and surface characteristics. To understand orientation behavior of particles in thin and thick films, we have used an order parameter, S, which is defined as

$$S = \left\langle \frac{3\cos^2\theta - 1}{2} \right\rangle, \tag{7}$$

where θ is the angle between z axis, unit vector normal to the surface, and the associating site of the molecule. The nature of orientation profiles (see Fig. 8) for thick and thin films are similar in nature but different in magnitude. Particles in the thick film are more oriented than in the thin film. Particles in the first molecular layer near the surface have relatively more tendency of orientation parallel to the surface. Increase in the association has more effect on the orientation of particles in the thick film compared to the thin film for a given temperature, which is due to increase in the density in thick film and decrease in the density of the thin film with increasing association. Nonetheless, the orientational order of the current system is substantially less to claim it to have significant anisotropic behavior. Hence, the orientation nature of the associating fluids with association strength $\varepsilon_{af}<=10$, perhaps, can be practically considered as isotropic in nature. We expect the above behavior and in general prewetting nature of associating fluids to change substantially if the surface contains association sites. We reserve this work for a future study.

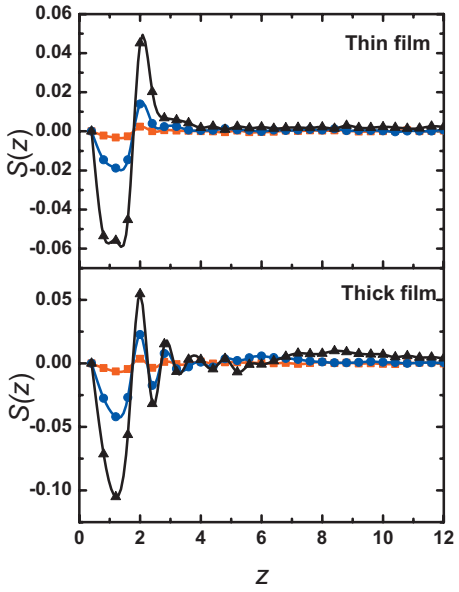

FIG. 8. Orientational order profile of coexistence thin and thick films at $T=0.85$ for different association strengths. Symbols square, circle and triangle represent $\varepsilon_{af}=4$, 6, and 8, respectively.

B. Prewetting critical and wetting temperature

Prewetting transition stems from the saturation curve at the wetting temperature, which is defined as the temperature corresponding to the transition from the partial wetting regime to the complete wetting regime. A generic method to obtain wetting temperature, with or without the existence of prewetting temperature, is to get contact angles for a series of temperatures. The temperature at which contact angle approaches zero is termed as wetting temperature. In this work, however, we have evaluated the difference between the bulk saturation chemical potential and prewetting chemical potential, $\Delta\mu$, for a series of temperatures and extrapolated it to zero to determine the wetting temperature. Prewetting critical temperature calculation is relatively trickier for thin-thick films as simple approaches which are widely used for bulk vapor-liquid phase transitions are not applicable.[62] Baxter[63] in his classical book describes the relation of boundary tension and critical temperature, which clearly suggest that boundary tension or free-energy barrier between thick and thin films should vanish at prewetting critical temperature. True or infinite size boundary tension is obtained by finite size scaling approach as described in the next section. In this work, we extrapolated a series of true boundary tension as a function of temperature to zero by fitting a second order polynomial function to get the prewetting critical temperature. Similar method has been used by earlier workers.[50]

Figure 9 presents the difference of bulk saturation and prewetting chemical potential, $\Delta\mu$, as a function of temperature. Theoretically,[64] it is argued that $\Delta\mu$ scales as $(T-T_w)^{3/2}$ for surface potential with van der Waals tail $\sim 1/z^3$. We linearly fitted, $\Delta\mu^{2/3}$ against $(T-T_w)$ to obtain the wetting temperature as shown in Fig. 9, and the values for different associating strengths are listed in Table I. Wetting temperature is seen to increase with increasing association strength. The behavior of wetting temperature for associating fluids is similar to that observed by the DFT.[52] Though, both

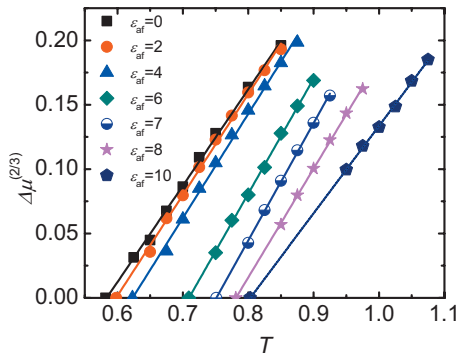

FIG. 9. Difference of bulk saturation chemical potential and prewetting chemical potential vs temperature for one site associating fluids.

wetting temperature and prewetting temperature are found to increase with increasing energy of association, the relative increase of T_w is higher than that of T_{pwc} with respect to bulk critical temperature, leading to shrinkage of the length of prewetting line, $(T_{pwc}-T_w)/T_{bc}$, with increase in the association strength. While, increase in the association to $\varepsilon_{af}=8$, led to significant jump in T_w and T_{pwc}, yet relative increase in these temperatures are similar; but, with respect to the bulk critical temperature, change in association to $\varepsilon_{af}=8$ decreases the length of the prewetting line. Further, increase in the association, $\varepsilon_{af}=10$, increases the prewetting critical temperature relatively larger than that in the wetting temperature, along with the bulk critical temperature, which effectively increases considerably the length of prewetting line. This behavior apparently has not been noticed by earlier workers using DFT.[52]

Bonn and Ross[33] provided an order of magnitude estimate of the distance between the prewetting line and bulk coexisting line based on few experimental results and presented in the form of

$$-\Delta\mu(T)/k_BT_w \cong \alpha[(T-T_w)/T_w]^{\beta}, \tag{8}$$

where α and β are approximately 0.5 and 1.5, as per Bonn and Ross's experimental observations. The exponent β is found to be 3/2 from theoretical calculation of Schick and Toberak[65] for fluid-wall interaction potential $\sim z^{-3}$. On the other hand, there is no theoretical estimate for α and hence, α can be different from the above approximate value for non-associating systems. Figure 10 presents Eq. (8) for vari-

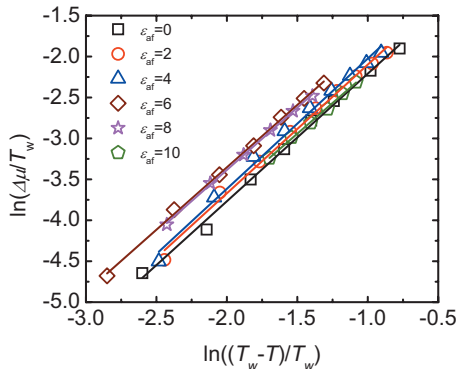

FIG. 10. Difference of bulk saturation chemical potential and prewetting chemical potential vs temperature in a scaled form as per Eq. (8).

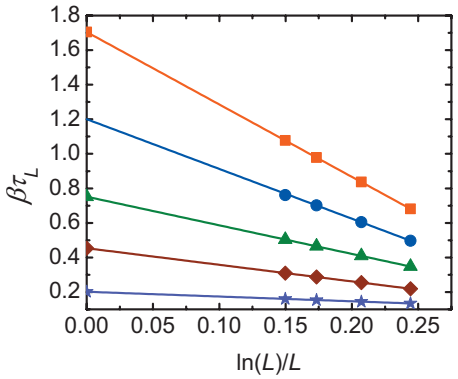

FIG. 11. System size dependence of the boundary tension for $\varepsilon_{af}=6.0$. Data points from top to bottom are from $T=0.8$ through $T=0.90$ in increments of 0.025. Lines provide an extrapolation to the infinite system size.

ous association energies on a log-log scale. The exponent, α, increase with increasing associating strength up to $\varepsilon_{af}=6$. Subsequently, it decreases with increase in associating strength; whereas β remains constant ~ 1.5 as expected for 9–3 substrate potential.[33] Similar behavior is seen for α in various experimental systems where it is found to vary from 0.4 to 0.6. For example, α is ~ 0.62 for H_2 on Cs,[66] ~ 0.56 for H_2 on Rb,[67] and ~ 0.42 for methanol on cyclohexane.[68] In addition, Bonn and Ross observed $-\Delta\mu(T_{PWC})/T_W \cong 0.03$; however, for the current system we observed this value within 0.1–0.15, which may be due to associating nature of the system.

C. Prewetting boundary tension

Binder's formalism, Eq. (5), is used to extrapolate the finite size thin-thick interfacial free-energy, obtained from a series of simulations with different substrate surface areas, to infinite length to get the true boundary tension. Typical finite size scaling plot for boundary tension calculation is shown in Fig. 11. The detailed description of calculating prewetting boundary tension is given elsewhere.[50] Boundary tensions of different associating fluids are presented in Fig. 12. As expected, boundary tension decreases with increase in the temperature and approaches zero at prewetting critical temperature. At a given temperature, boundary tension increases with the increase in the association strength akin to behavior of vapor-liquid surface tension of bulk associating fluids.[58] The inset of Fig. 12 presents the boundary tension of different associating system as a function of reduced temperature. At a constant T/T_{pwc}, boundary tension increases with increasing associating strength up to 8. Subsequent increase in the association strength drastically reduces the boundary tension as noticed for $\varepsilon_{af}=10$. Interestingly, this behavior is also seen for surface tension of bulk associating fluids.[58] This behavior is mainly attributed to substantial change in the molecular arrangement in the thin and thick films, which in effect reduces the interfacial free-energy of the system dramatically. We believe that similar behavior could exist for molecular systems for two and four site associating fluids, which we plan to study in near future. In addition, the current simulations are envisaged to help DFT and other theoretical methods particularly in search for prewetting transition of molecular systems.

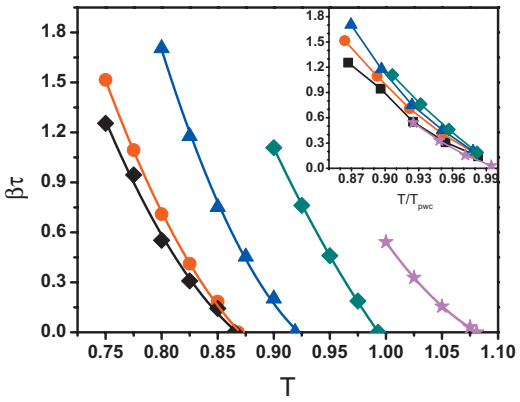

FIG. 12. Infinite system size boundary tension vs temperature for various association strengths. Curves serve as a guide to the eye. The inset represents the infinite system size boundary tension vs reduced temperature for different associating strengths. Symbols square, circle, triangle, diamond and star represent boundary tension for associating strength $\varepsilon_{af}=2$, 4, 6, 8, and 10, respectively.

V. CONCLUSION

We have studied the influence of associating strength on prewetting phase transition, monomer fraction, orientation profile, and boundary tension of dimer forming associating fluids. Wetting and prewetting temperature increases with increasing associating strength. Prewetting temperatures with respect to the bulk critical temperature, T_{pwc}/T_{bc}, found in numerous experiments and simulations, are in a wide range. For example, T_{pwc}/T_{bc} is ~ 0.672 for Ne on Mg,[69] ~ 0.786 for Ar on CO_2,[49] ~ 0.90 for Ne on CO_2,[70] ~ 0.99 for Hg on sapphire[71] and ~ 1.05 for Hg on molybdenum.[72] On the other hand, T_w/T_{bc} for molecular systems such as water, described by the TIP4P model,[54] on various substrate described by a 9–3 LJ potential was found to be in the range of 0.986–0.998. Zhao recently performed GCMC based simulations for SPC/E model of water on graphite for which T_w/T_{bc} and T_{pwc}/T_{bc} were found to be ~ 0.75 and ~ 0.8, respectively. Similar values of T_w/T_{bc} (~ 0.72) and T_{pwc}/T_{bc} (~ 0.8) were observed experimentally for acetone on graphite.[40] In the current study, T_w/T_{bc} and T_{pwc}/T_{bc} are in the range of $\sim 0.505-0.605$ and $\sim 0.727-0.814$, respectively These values, however, are not in agreement convincingly with that seen for molecular systems. Perhaps, the disagreement is due to the dimer-forming model considered in the current study, which cannot be used for water or acetone.

The current results are in agreement with the DFT's results at lower association strengths. At higher association, we observed a complex behavior which has not earlier seen/predicted by the DFT. Length of prewetting line is seen to decreases with increasing association strength until $\varepsilon_{af}=8$ and subsequently it increase substantially as seen for $\varepsilon_{af}=10$. This behavior is in disagreement with the DFT study and also raises a question of second order transition (i.e., zero prewetting length) at higher association strength as predicted by the DFT. However, at a weaker substrate potential it is expected to show second order transition as shown by Sellers and Errington.[73] The current system with the surface

fluid interaction parameters does not display any layering transition as also observed in the DFT study.[52] However, layering transitions are expected at higher substrate potentials, as seen in the water study of Brovchenko and co-workers[53,54] in cylindrical and slit pores.

Boundary tension using finite size scaling is reported for associating fluids. Interestingly, boundary tension behavior is seen similar to that of bulk vapor-liquid surface tension of associating fluids. Boundary tension at a reduced temperature is seen to be maximum for $\varepsilon_{af}=8$. Substantial drop in boundary tension is observed, at a reduced temperature, for $\varepsilon_{af}=10$, which is due to the significant structural change in the thin film compared to that in the thick film.

ACKNOWLEDGMENTS

We thank Peter Cummings for many helpful discussions. This work was supported by the Department of Science and Technology, Government of India (Grant No. IR/S3/EU/005/2007)

[1] M. Wertheim, J. Stat. Phys. **35**, 19 (1984).
[2] M. Wertheim, J. Stat. Phys. **35**, 35 (1984).
[3] W. G. Chapman, J. Chem. Phys. **93**, 4299 (1990).
[4] E. Müller and K. E. Gubbins, Ind. Eng. Chem. Res. **40**, 2193 (2001).
[5] G. Jackson, W. G. Chapman, and K. E. Gubbins, Mol. Phys. **65**, 1 (1988).
[6] J. K. Johnson and K. E. Gubbins, Mol. Phys. **77**, 1033 (1992).
[7] S. H. Huang and M. Radosz, Ind. Eng. Chem. Res. **29**, 2284 (1990).
[8] S. H. Huang and M. Radosz, Ind. Eng. Chem. Res. **30**, 1994 (1991).
[9] D. G. Green and G. Jackson, J. Chem. Soc., Faraday Trans. **88**, 1395 (1992).
[10] J. Kolafa and I. Nezbeda, Fluid Phase Equilib. **100**, 1 (1994).
[11] T. Kraska and K. E. Gubbins, Ind. Eng. Chem. Res. **35**, 4727 (1996).
[12] T. Kraska and K. E. Gubbins, Ind. Eng. Chem. Res. **35**, 4738 (1996).
[13] M. Banaszak, C. K. Chen, and M. Radosz, Macromolecules **29**, 6481 (1996).
[14] F. J. Blas and L. F. Vega, Ind. Eng. Chem. Res. **37**, 660 (1998).
[15] J. C. Pàmies and L. F. Vega, Ind. Eng. Chem. Res. **40**, 2532 (2001).
[16] A. Gil-Villegas, A. Galindo, P. J. Whitehead, S. J. Mills, G. Jackson, and A. N. Burgess, J. Chem. Phys. **106**, 4168 (1997).
[17] A. Galindo, A. Gil-Villegas, G. Jackson, and A. N. Burgess, J. Phys. Chem. B **103**, 10272 (1999).
[18] H. Adidharma and M. Radosz, Fluid Phase Equilib. **161**, 1 (1999).
[19] J. Gross and G. Sadowski, Ind. Eng. Chem. Res. **40**, 1244 (2001).
[20] F. J. Blas, E. M. del Rio, E. de Miguel, and G. Jackson, Mol. Phys. **99**, 1851 (2001).
[21] G. J. Gloor, G. Jackson, and F. J. Blas, J. Phys. Chem. C **111**, 15513 (2007).
[22] D. P. Visco, Jr. and D. A. Kofke, J. Chem. Phys. **110**, 5493 (1999).
[23] B. Chen and J. I. Siepmann, J. Phys. Chem. B **104**, 8725 (2000).
[24] S. Wierzchowski and D. A. Kofke, J. Chem. Phys. **114**, 8752 (2001).
[25] J. Alejandre, Y. Duda, and S. Sokolowski, J. Chem. Phys. **118**, 329 (2003).
[26] P. Orea, J. Chem. Phys. **123**, 144704 (2005).
[27] T. Li and E. Nies, J. Phys. Chem. B **111**, 8131 (2007).
[28] N. Kern and D. Frenkel, J. Chem. Phys. **118**, 9882 (2003).
[29] F. Sciortino, E. Bianchi, J. F. Douglas, and P. Tartaglia, J. Chem. Phys. **126**, 194903 (2007).
[30] Z. Zhang and S. C. Glotzer, Nano Lett. **4**, 1407 (2004).
[31] K. E. Sung, S. A. Vanapalli, D. Mukhija, H. A. Mckay, J. M. Millunchick, M. A. Burns, and M. J. Soloman, J. Am. Chem. Soc. **130**, 1335 (2008).
[32] L. D. Gelb, K. E. Gubbins, R. Radhakrishnan, and M. S. Bartkowiak, Rep. Prog. Phys. **62**, 1573 (1999).
[33] D. Bonn and D. Ross, Rep. Prog. Phys. **64**, 1085 (2001).
[34] J. W. Cahn, J. Chem. Phys. **66**, 3667 (1977).
[35] C. Ebner and W. F. Saam, Phys. Rev. Lett. **38**, 1486 (1977).
[36] J. E. Rutledge and P. Taborek, Phys. Rev. Lett. **69**, 937 (1992).
[37] R. B. Hallock, J. Low Temp. Phys. **101**, 31 (1995).
[38] J. A. Phillips, D. Ross, P. Taborek, and J. E. Rutledge, Phys. Rev. B **58**, 3361 (1998).
[39] E. Cheng, G. Mistura, H. C. Lee, M. H. W. Chan, M. W. Cole, C. Carraro, W. F. Saam, and F. Toigo, Phys. Rev. Lett. **70**, 1854 (1993).
[40] F. Kruchten and K. Knorr, Phys. Rev. Lett. **91**, 085502 (2003).
[41] J. E. Finn and P. A. Monson, Phys. Rev. A **39**, 6402 (1989).
[42] W. Shi, X. Zhao, and J. Johnson, Mol. Phys. **100**, 2139 (2002).
[43] M. B. Sweatman, Phys. Rev. E **65**, 011102 (2001).
[44] M. J. P. Nijmeijer, C. Bruin, and A. F. Bakker, Mol. Phys. **72**, 927 (1991).
[45] J.-S. Wang and R. H. Swendsen, J. Stat. Phys. **106**, 245 (2002).
[46] J. R. Errington, Phys. Rev. E **67**, 012102 (2003).
[47] B. A. Berg and T. Neuhaus, Phys. Rev. Lett. **68**, 9 (1992).
[48] A. M. Ferrenberg and R. H. Swendsen, Phys. Rev. Lett. **61**, 2635 (1988).
[49] J. R. Errington, Langmuir **20**, 3798 (2004).
[50] J. R. Errington and D. W. Wilbert, Phys. Rev. Lett. **95**, 226107 (2005).
[51] M. Borówko, A. Patrykiejew, S. Sokolowski, and R. Zagorski, J. Chem. Soc., Faraday Trans. **94**, 771 (1998).
[52] A. Patrykiejew and S. Sokolowski, J. Phys. Chem. B **103**, 4466 (1999).
[53] I. Brovchenko, A. Greiger, and A. Oleinikova, J. Chem. Phys. **120**, 1958 (2004).
[54] I. Brovchenko and A. Oleinikova, J. Phys. Chem. C **111**, 15716 (2007).
[55] X. Zhao, Phys. Rev. B **76**, 041402 (2007).
[56] J. K. Singh, G. Sarma, and S. K. Kwak, J. Chem. Phys. **128**, 044708 (2008).
[57] A. Saha, S. P. Singh, J. K. Singh, and S. K. Kwak, Mol. Phys. **107**, 2189 (2009).
[58] J. K. Singh and D. A. Kofke, J. Chem. Phys. **121**, 9574 (2004).
[59] R. Pandit, M. Schick, and M. Wortis, Phys. Rev. B **26**, 5112 (1982).
[60] K. Binder, Phys. Rev. A **25**, 1699 (1982).
[61] J. K. Singh and D. A. Kofke, Mol. Simul. **30**, 343 (2004).
[62] J. K. Singh, D. A. Kofke, and J. R. Errington, J. Chem. Phys. **119**, 3405 (2003).
[63] R. J. Baxter, *Exactly Solved Models in Statistical Mechanics* (Academic, New York, 1982).
[64] F. Ancilotto and F. Toigo, Phys. Rev. B **60**, 9019 (1999).
[65] M. Schick and P. Taborek, Phys. Rev. B **46**, 7312 (1992).
[66] D. Ross, P. Taborek, and J. E. Rutledge, Phys. Rev. B **58**, R4274 (1998).
[67] G. Mistura, H. C. Lee, and M. H. W. Chan, J. Low Temp. Phys. **96**, 221 (1994).
[68] H. Kellay, D. Bonn, and J. Meunier, Phys. Rev. Lett. **71**, 2607 (1993).
[69] M. J. Bojan, G. Stan, S. Curtarolo, W. A. Steele, and M. W. Cole, Phys. Rev. E **59**, 864 (1999).
[70] F. Ancilotto and F. Toigo, J. Chem. Phys. **112**, 4768 (2000).
[71] Y. Ohmasa, Y. Kajihara, and M. Yao, Phys. Rev. E **63**, 051601 (2001).
[72] V. F. Kozhevnikov, D. I. Arnold, S. P. Naurzakov, and M. E. Fisher, Phys. Rev. Lett. **78**, 1735 (1997).
[73] M. S. Sellers and J. R. Errington, J. Phys. Chem. C **112**, 12905 (2008).